Special Issue Article

Advances in Mechanical Engineering

Advances in Mechanical Engineering
2018, Vol. 10(3) 1–11

DOI: 10.1177/1687814018763411
journals.sagepub.com/home/ade
SAGE

A compensation method based on extreme learning machine to enhance absolute position accuracy for aviation drilling robot

Peijiang Yuan[1], Dongdong Chen[1], Tianmiao Wang[1], Shuangqian Cao[1], Ying Cai[1] and Lei Xue[2]

Abstract

To enhance the absolute position accuracy and solve complex modeling and computational complexity problems in traditional compensation methods for aviation drilling robots, a compensation method based on the extreme learning machine model was proposed in this article. The proposed method, in which the influence of geometric factors and the non-geometric factors of the robot is considered, builds a positional error prediction model based on extreme learning machine. As the input and output training data, the theoretical position and positional errors measured by a high-precision laser tracker were used to train and construct the extreme learning machine model. After the extreme learning machine model was constructed, the positional errors of prediction points could be predicted using the trained extreme learning machine. Then, the drilling robot controller could be directed to compensate for the predicted positional errors. To verify the correctness and effectiveness of the method, a series of experiments were performed with an aviation drilling robot. The experimental results showed that choosing an appropriate number of training points and hidden neurons for extreme learning machine could increase the computational efficiency without decreasing the high absolute position accuracy. The results also show that the average and maximum absolute position accuracy of robot tool center point were improved by 75.89% and 80.93%, respectively.

Keywords

Robot compensation, absolute positional error, positional error prediction, extreme learning machine, drilling robot

Date received: 1 July 2017; accepted: 7 February 2018

Handling Editor: Chenguang Yang

Introduction

Aircraft assembly is one of the most important aspects of aircraft production and accounts for approximately half of the total aircraft manufacturing workload. The quality of aircraft assembly directly affects the life of the aircraft structure. The connection between the parts in aircraft assembly is based on riveting and bolting. Drilling is an important process before riveting and bolting, and the current form of drilling is primarily manual; however, the drilling hole quality and connection quality do not meet the quality requirements of high-performance aircraft.[1–3] The application of aviation drilling robots can greatly improve the quality of the hole and the quality of the connection.[4] In addition,

[1]School of Mechanical Engineering and Automation, Beihang University, Beijing, China
[2]Shanghai Aircraft Manufacturing Co., Ltd, Shanghai, China

Corresponding author:
Peijiang Yuan, School of Mechanical Engineering and Automation, Beihang University, Beijing 100191, China.
Email: itr@buaa.edu.cn

these robots can improve the passing rate of the product. Repeatability and absolute accuracy, important indices of aviation drilling robots' positioning accuracy, are the basis of all processes. The aviation drilling robot consists mainly of the end effector and the robotic manipulator. The end effector is attached to the flange of the robotic manipulator. Thus, positional accuracy is determined primarily by the robotic manipulator. Current robotic manipulators generally achieve high repeatability. For example, the repeatability of a KUKA KR210 can reach ± 0.06 mm, whereas the absolute accuracy is only ± 3 mm. The absolute accuracy cannot meet the accuracy requirement of ± 0.5 mm in aircraft assembly.[5,6] An increasing number of aviation drilling robots are operated by offline programming.[2,7] Generally, drilling robots with only high repeatability are not adequate for high-end manufacturing, which also requires high absolute accuracy.[8] Thus, high absolute accuracy has been pursued by researchers internationally.[9–20]

Sources leading to a loss of absolute accuracy are usually concurrent. Errors caused by link length, nonparallel axes, base misalignment, manufacturing errors, and assembly errors are classified as geometric errors and account for approximately 90% of all errors. The other 10% of errors are caused by the payload, thermal deflection, gear backlash, servo error, and so on, and they are called non-geometric errors.[12,13] Therefore, studies have considered geometric errors for calibration, while non-geometric errors have been ignored.[14,15]

Two types of compensation methods have been developed: model-based compensation and model-free compensation.[16] In the model-based compensation method, errors of kinematic parameters are identified based on the kinematic model, which is constructed first. A Denavit–Hartenberg (DH) model is a convenient method for determining the deviation of kinematic parameters.[17,18] When adjacent axes are parallel, the solution will be singular. To solve this problem, a modified Denavit–Hartenberg (MDH) model is proposed. Compared with a DH model, a MDH model adds an additional parameter representing the rotation around the y axis.[15,19] An S-model that has six parameters can also overcome the singularity problem of the DH model.[20–22] A parameter identification method based on the S-model is proposed.[22] The product-of-exponential (POE) model can be used to construct the kinematic model of a robot.[23] He et al.[24] proposed a parameter identification method for robot calibration based on POE. In model-based compensation, in addition to modeling, parameter identification is another difficulty. The linear least squares method,[25] non-linear optimization procedure,[26,27] iterative linearization,[28] extended Kalman filter,[15,27–29] and Levenberg–Marquardt[30] are all algorithms for parameter identification. The model-based methods generally ignore small errors when modeling, which results in non-ideal compensation accuracy. The model-based methods are not universal for all types of robots and have the problems associated with complex modeling and computational complexity.

Another type of compensation method, the model-free method, holds that position errors and robot joint values or robot positions are correlated. A number of approaches, such as Fourier polynomial,[31,32] inverse distance weighting,[33] kriging,[16] and artificial neural network (ANN),[15,34,35] have been utilized to predict position errors. However, Fourier polynomial is limited because of its low accuracy and high complexity. Inverse distance weighting is only applicable when the movement of the robot space is in a small range. The kriging method is complex, and it is challenging for field engineers to master.

Compared with the methods mentioned above, the ANN method, which has high learning ability and high adaptability, can constantly adjust the weight of the associated node so that the output can approach the desired results. Therefore, the ANN method has been rapidly developed to provide higher precision for industrial robots. Single-hidden-layer forward neural network (SLFN) is a traditional ANN that has been widely used.[36] However, the SLFN method is limited by slow training, the difficulty of obtaining a global optimal solution, and the difficulty of choosing a learning rate. To solve these problems, the extreme learning machine (ELM) algorithm has been proposed by Huang et al.[37,38] Compared with the ordinary SLFN, the ELM algorithm, which presents improved generalization, simplifies the training without iteration. In addition, ELM can be used to compensate the unknown nonlinearity for industrial robot, which is a non-linear system, and has the advantage of high efficiency.[39]

A novel compensation method based on ELM was proposed to improve the absolute position accuracy and solve the problem of complex modeling and computational complexity. The method does not need to construct a kinematics model of the robot and identify the kinematic parameters. Considering the influence of the geometric factors and the non-geometric factors of the aviation drilling robot, the proposed method built a positional error prediction model based on ELM. As the input and output training data, the theoretical position and positional errors measured by a high-precision laser tracker were used to train and construct the ELM model. After the ELM model was constructed, the positional errors of prediction points could be predicted using the trained ELM. Then, the drilling robot controller could compensate for the predicted positional errors.

The rest of the article is organized as follows: section "Compensation principle" describes the compensation principle based on ELM; section "Experimental results

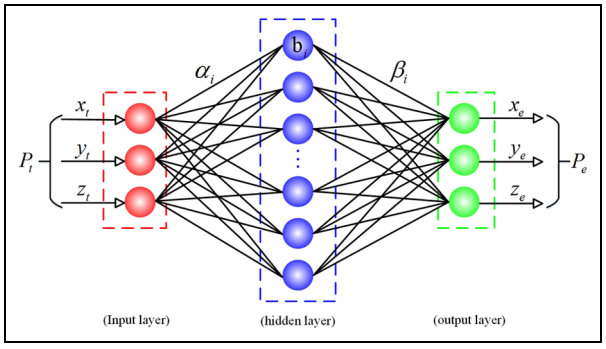

Figure 1. Structure of ELM.

and analysis" presents the experiments and analysis of the results for the aviation drilling robot; and section "Conclusion" discusses the conclusions.

Compensation principle

ELM principle

The drilling robot tool center point (TCP) is used as the research object to study compensation in this article.Figure 1 shows the structure of a three-layer ELM. The theoretical position $P_t(x_t\ y_t\ z_t)$ of the robot TCP is the input of the ELM, which consists of three nodes. The three nodes in the input layer represent the three elements of the theoretical position vector $\boldsymbol{P_t} = [x_t,\ y_t,\ z_t]^T$. The hidden layer is composed of k neurons. A sum function is used as the activating function of the neurons. The positional error $P_e(x_e,\ y_e,\ z_e)$ in theoretical position $P_t(x_t,\ y_t,\ z_t)$ is the output of the ELM, which is composed of three neurons. The three neurons in the output layer represent the three elements of the positional error vector $\boldsymbol{P_e} = [x_e,\ y_e,\ z_e]^T$. The absolute positional error can be expressed as follows

$$\boldsymbol{e} = \sqrt{x_e^2 + y_e^2 + z_e^2} \tag{1}$$

Given N different learning sample pairs $\boldsymbol{P_{tj}}$ and $\boldsymbol{P_{ej}}$, where $\boldsymbol{P_{tj}}$ belongs to R^3 and $\boldsymbol{P_{ej}}$ belongs to R^3, the output of ELM with k hidden neurons can be described as follows

$$f(\boldsymbol{P_{tj}}) = \sum_{i=1}^{k} \boldsymbol{\beta_i} G_i(\boldsymbol{\alpha_i}, b_i, \boldsymbol{P_{tj}}), \quad j = 1, 2, \ldots, N \tag{2}$$

where $\boldsymbol{\alpha}_i$ is the input weights of the ith hidden neuron, b_i is the threshold of the ith hidden neuron, and $\boldsymbol{\beta_i}$ is the output weights connecting the ith hidden neuron and the output layer. $\boldsymbol{P_{tj}}$, $\boldsymbol{P_{ej}}$, $\boldsymbol{\alpha_i}$ and $\boldsymbol{\beta_i}$ are defined as

$$\boldsymbol{P_{tj}} = [x_{tj}, y_{tj}, z_{tj}]^T \tag{3}$$

$$\boldsymbol{P_{ej}} = [x_{ej}, y_{ej}, z_{ej}]^T \tag{4}$$

$$\boldsymbol{\alpha_i} = [\alpha_{i1}, \alpha_{i2}, \alpha_{i3}]^T \tag{5}$$

$$\boldsymbol{\beta_i} = [\beta_{i1}, \beta_{i2}, \beta_{i3}]^T \tag{6}$$

In addition, G_i ($\boldsymbol{\alpha_i}$, b_i, $\boldsymbol{P_{tj}}$) represents the output of the ith hidden neuron that is associated with $\boldsymbol{P_{tj}}$. ELM can be divided into two types: a sum function as the hidden function or a radical basis function as the hidden function. In this article, the sum function is the hidden function. G_i ($\boldsymbol{\alpha_i}$, b_i, $\boldsymbol{x_j}$) is calculated as follows

$$G(\boldsymbol{\alpha_i}, b_i, \boldsymbol{P_{tj}}) = g(\boldsymbol{\alpha_i P_{tj}} + b_i) \tag{7}$$

where g is the activating function of the hidden neurons.

The ELM searches for the optimal pairs $\boldsymbol{W}$ (i.e. $\boldsymbol{\alpha}^*$, $\boldsymbol{b}^*$, and $\boldsymbol{\beta}^*$) that lead to the smallest $E(\boldsymbol{W})$ in equation (7), which is the sum of the squares of errors between the expected and actual values

$$E(\boldsymbol{W}) = \sum_{j=1}^{N} (f(\boldsymbol{P_{tj}}) - \boldsymbol{P_{ej}})^2 \tag{8}$$

The matrix form of equation (2) can be written as follows

$$\boldsymbol{H\beta} = \boldsymbol{T} \tag{9}$$

where $\boldsymbol{H}$ is the output matrix of the hidden layer, whose ith column shows the output of all the N input samples associated with the ith hidden neuron. In addition, $\boldsymbol{H}$ is defined as shown in equation (10), and matrices $\boldsymbol{\beta}$ and $\boldsymbol{T}$ are presented in the order of equations (11) and (12)

$$\boldsymbol{H} = \begin{bmatrix} G(\boldsymbol{\alpha_1}, b_1, \boldsymbol{P_{t1}}) & \cdots & G(\boldsymbol{\alpha_k}, b_k, \boldsymbol{P_{t1}}) \\ G(\boldsymbol{\alpha_1}, b_1, \boldsymbol{P_{t2}}) & \cdots & G(\boldsymbol{\alpha_k}, b_k, \boldsymbol{P_{t2}}) \\ \vdots & \cdots & \vdots \\ G(\boldsymbol{\alpha_1}, b_1, \boldsymbol{P_{tN}}) & \cdots & G(\boldsymbol{\alpha_k}, b_k, \boldsymbol{P_{tN}}) \end{bmatrix}_{N \times k} \tag{10}$$

$$\boldsymbol{\beta} = \begin{bmatrix} \boldsymbol{\beta}_1^T & \boldsymbol{\beta}_2^T & \cdots & \boldsymbol{\beta}_k^T \end{bmatrix}^T_{k \times 3} \tag{11}$$

$$\boldsymbol{T} = \begin{bmatrix} \boldsymbol{P_{e1}^T} & \boldsymbol{P_{e2}^T} & \cdots & \boldsymbol{P_{eN}^T} \end{bmatrix}^T_{N \times 3} \tag{12}$$

ELM specifies the number of the hidden neurons (i.e. k) and assigns the learning parameter pairs of the hidden neurons (i.e. $\boldsymbol{\alpha_i}$ and b_i) randomly. This definition indicates that the connection weights of the hidden neurons (i.e. $\boldsymbol{\beta}$) can be directly solved without iterations by the following equation

$$\boldsymbol{\beta} = \boldsymbol{H}^+ \boldsymbol{T} \tag{13}$$

where $\boldsymbol{H}^+$ is a Moore–Penrose generalized inverse matrix, which can be expressed as follows

$$\boldsymbol{H}^+ = \left(\boldsymbol{H}^T \boldsymbol{H}\right)^{-1} \boldsymbol{H}^T \tag{14}$$

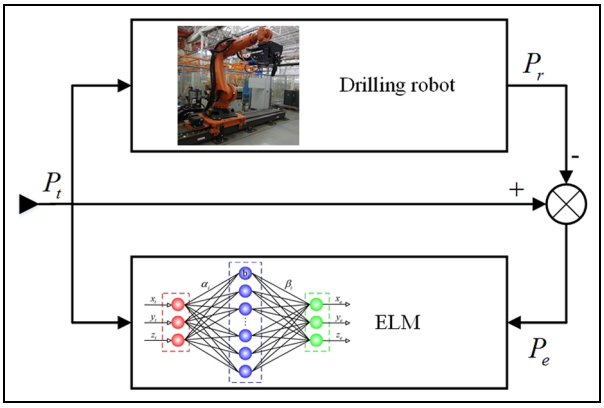

Figure 2. ELM training.

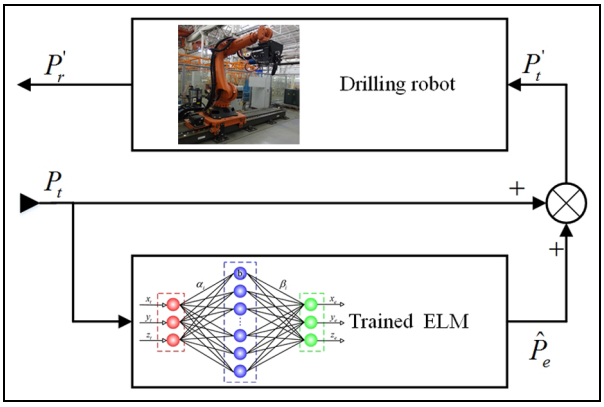

Figure 3. Compensation of the positional error.

After the matrix $\boldsymbol{\beta}$ is obtained, the ELM for the positional error prediction model is constructed.

The illustration of the ELM training process is shown in Figure 2. The theoretical position $\boldsymbol{P_t}$ of robot TCP is used as the input data of the drilling robot. The output data of the drilling robot is the real position $\boldsymbol{P_r}$. The positional error $\boldsymbol{P_e}$ can be expressed as follows

$$\boldsymbol{P_e} = \boldsymbol{P_t} - \boldsymbol{P_r} \tag{15}$$

where $\boldsymbol{P_t}$ and $\boldsymbol{P_e}$ are the input training data and output training data of ELM, respectively.

Positional error compensation

The compensation process of positional errors for a drilling robot is described in Figure 3. After the ELM is trained, the theoretical position $\boldsymbol{P_t}$ of the prediction point is the input data of the trained ELM, and the output data is the prediction positional error $\hat{\boldsymbol{P}}_e$ of the corresponding prediction point. With respect to error compensation, because the error prediction above does not rely on the kinematic model, the kinematic parameters have not been modified. In this study, error compensation is performed by compensating the position coordinates given to the drilling robot. Position compensation after error identification is presented as follows

$$\boldsymbol{P'_t} = \boldsymbol{P_t} + \hat{\boldsymbol{P}}_e \tag{16}$$

where $\boldsymbol{P'_t}$ represents the position coordinates after compensation.

To reach the specified location, the controller would give the drilling robot the position coordinates $\boldsymbol{P'_t}$ and not the desired position coordinates. $\boldsymbol{P'_r}$ is the real position co-ordinate of the drilling robot after compensation.

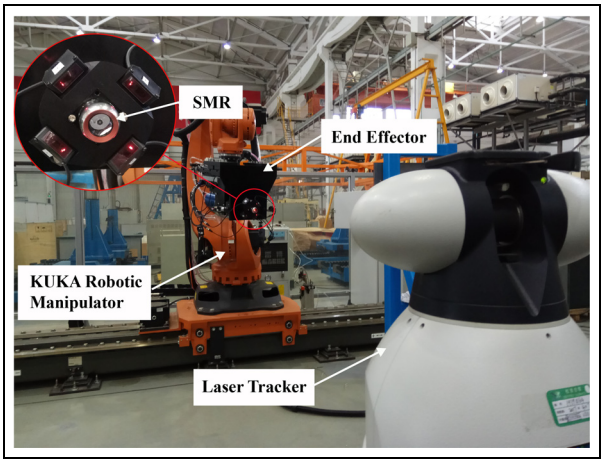

Figure 4. Setup of an experimental compensation system.

Experimental results and analysis

As shown in Figure 4, the practical compensation of an aviation drilling robot is used to verify the compensation method in this article. The experimental setup consists of a KUKA KR210 R2700 robotic manipulator, an end effector, a laser tracker, and an accompanying spherically mounted reflector (SMR). The end effector is attached to the flange of the robotic manipulator. The spherical center of the SMR attached to the end effector is on the spindle axis of the end effector, as shown in Figure 4. The spherical center of the SMR is regarded as the drilling robot TCP. The KUKA KR210 R2700 robotic manipulator and drilling end effector are the key parts of the aviation drilling robot. The robotic manipulator is a 6-degree-of-freedom (DOF) serial manipulator. The repetitive positioning accuracy of the robotic manipulator is ± 0.06 mm, and its absolute positioning accuracy is not mentioned in the specification. The type of the laser tracker is a Leica AT901, and its absolute distance measuring accuracy is $7.5 + 3\,\mu m/m$.

Measuring TCP

The drilling robot TCP is used as the research object to study compensation in this article. The difference between the real computer-aided design (CAD) model and the ideal CAD model of the end effector leads to misalignment between the real TCP and theoretical TCP. Thus, the drilling robot TCP must be measured before compensation to obtain the position relation between the TCP and flange frame of the robot. A XYZ-4-points method is used to determine the TCP in this article. The principle of the XYZ-4-points method is that the robot TCP moves to the same point from four difference postures. The position parameters of the flange in four difference postures are calculated by the robot control system to obtain the robot TCP. The SMR cannot be close to a real reference point to measure the TCP in practice as shown in Figure 4; therefore, a virtual XYZ-4-points method in coordination with a laser tracker is used. A robot controlled by the control system moves so that the SMR is close to a virtual point from four different postures. When the positional error between the SMR and the virtual point is less than 0.02 mm (absolute distance measuring accuracy of the laser tracker in practice), the SMR is considered to coincide with the virtual point. Then, the robot TCP can be obtained by the robot control system.

Establishing the robot base frame

To obtain the absolute positioning accuracy, the robot's base frame must be established first. The positional errors of the robot TCP reflect the robot absolute positioning accuracy. Thus, the positional errors of robot TCP are measured in the robot base frame. In this article, spatial analyzer (SA) software developed by New River Kinematics, in coordination with a laser tracker, is used to establish the robot base frame and measure the position of the robot TCP in the robot base frame. Robotmaster software is applied to generate an offline program of the robot.

The robot base frame is established as follows:

1. L-type path, which consists of two lines, is designed to generate corresponding offline programming in Robotmaster, as shown in Figure 5. One of the two lines parallels the Y_B axis of the robot base frame, and another parallels the Z_B axis.
2. A set of TCP positions measured while moving along the Y_B axis positive direction is used to fit the Y_A axis, as shown in Figure 5.
3. When the TCP moves to the point O_A, the theoretical coordinate value of point O_A is recorded and measured with the SA software.

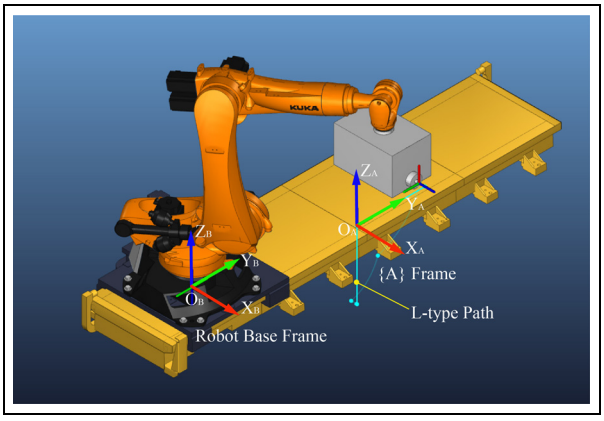

Figure 5. Establishing the robot base frame.

4. A set of TCP positions measured while moving along the Z_B axis negative direction is used to fit the Z_A axis.
5. Let us construct the {A} frame with its origin at the point O_A in which two fitted lines are the Y_A axis and Z_A axis, respectively, in SA software.
6. The {A} frame is constructed approximately parallel to the robot base frame. The {A} frame is translated in terms of the value recorded in equation (2), and the robot base frame is established.

Because of the measurement errors of the laser tracker, the line fitting errors and principle errors, the constructed robot base frame cannot absolutely coincide with the theoretical robot base frame. Therefore, a deviation is observed between the positional errors of the robot TCP measured in the constructed robot base frame and the theoretical positional errors. The deviation is the constructed error of the robot base frame. In practice, the target points are applied in the constructed robot base frame, and the compensation of the robot TCP is also applied in the constructed robot base frame; thus, the constructed errors of the robot base frame have little effect on robot compensation.

Influencing factors of absolute position accuracy

The number of training samples and the number of nodes in the hidden layer are the important factors that influence the training effect of the neural network. Thus, the training effect of the ELM algorithm, one of the traditional neural networks, is influenced by the number of training points and the number of nodes in the hidden layer. To obtain the optimal parameters, a set of experiments are implemented.

Effect of the number of training points on absolute position accuracy. The training effect of the ELM is influenced

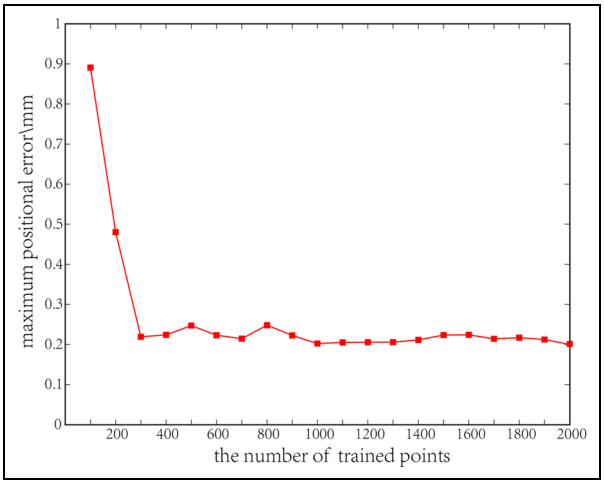

Figure 6. Effect of the number of training points on the maximum positional error.

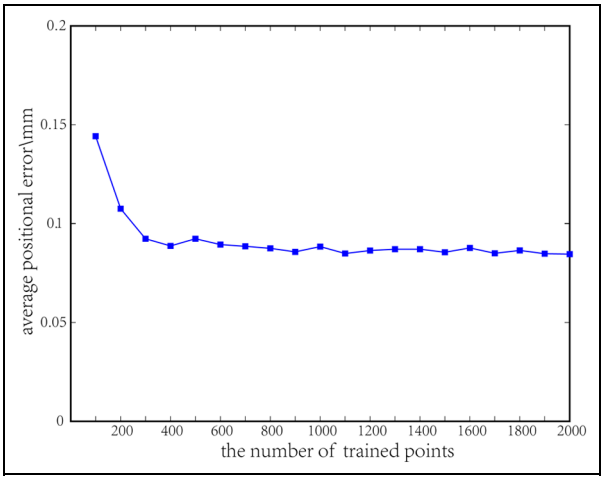

Figure 7. Effect of the number of training points on the average positional error.

by the number of training points. Thus, the training effect of the ELM has an impact on the absolute position accuracy of the robot. To obtain the relationship between the absolute position accuracy and the number of training points for the ELM, an experiment is performed on the aviation drilling robot.

According to the method mentioned above, the robot TCP is measured, and the robot base frame is established first. Subsequently, 2000 random points in the robot workspace are chosen, and they are evenly distributed in the robot workspace. The path of the robot TCP is designed in the Robotmaster software, and the corresponding offline program of the robot is generated. After the robot TCP moves to the samples, the real position of robot TCP can be measured using the laser tracker. Then, the real positional error of the 2000 points can be calculated. In addition, 100 random points, 200 random points, ..., 2000 random points from the 2000 measurement points mentioned above are chosen to train the ELM. The hidden layer is composed of 40 neurons. A sum function is used as the activating function of the ELM. After 20 ELM models are constructed, 150 random points are used to obtain absolute position accuracy using 20 ELM models. The experimental results are shown in Figures 6 and 7.

The maximum positional error and average positional error are two important indexes of absolute position accuracy. The experimental results show that when the number of training points is less than 300, the maximum positional error and average positional error reduce as the number of training points increase. When the number of training points is greater than 300, as the number of training points increase, the maximum positional error and average position error tend to be stable.

In real applications, more points for ELM training take more measurement time, training time, and workload. Choosing the appropriate number of training points for the ELM can ensure high absolute position accuracy and reduce the time and the amount of work.

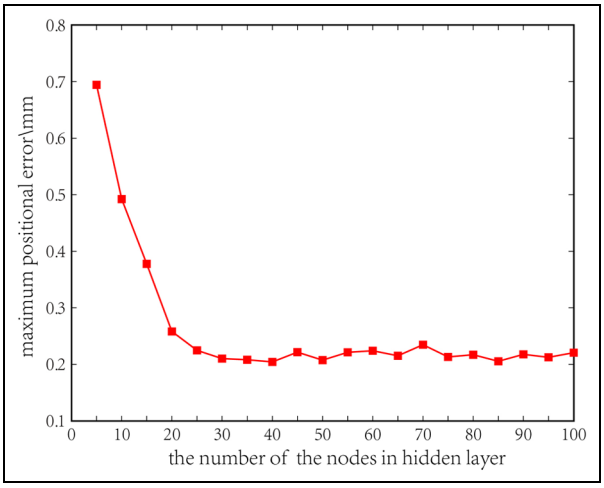

Figure 8. Effect of the number of the nodes in the hidden layer on the maximum position error.

Effect of the number of the nodes in the hidden layer on absolute position accuracy. The number of the nodes in the hidden layer is another important factor influencing the training effect of the ELM. In addition, 1000 random points from the 2000 measurement points above are selected for ELM training, and the numbers of nodes in the hidden layer are 5, 10, ..., 100. After 20 ELM models are constructed, 150 random points are used to obtain the absolute position accuracy using 20 ELM models. The experimental results are shown in Figures 8 and 9.

Table 1. Experimental results of the positional errors.

Direction		Range (mm)	Mean (mm)	Standard deviation (mm)
X	Before	[−0.3191, 0.7798]	0.0473	0.2266
	After	[−0.1200, 0.1174]	0.0016	0.0356
Y	Before	[−0.8062, 0.7645]	−0.1192	0.3067
	After	[−0.1582, 0.1858]	−0.0043	0.0640
Z	Before	[−0.2693, 0.4606]	0.0408	0.1669
	After	[−0.1335, 0.1516]	0.0017	0.0694
e	Before	[0.0851, 1.0207]	0.3816	0.2119
	After	[0.0119, 0.1946]	0.0920	0.0411

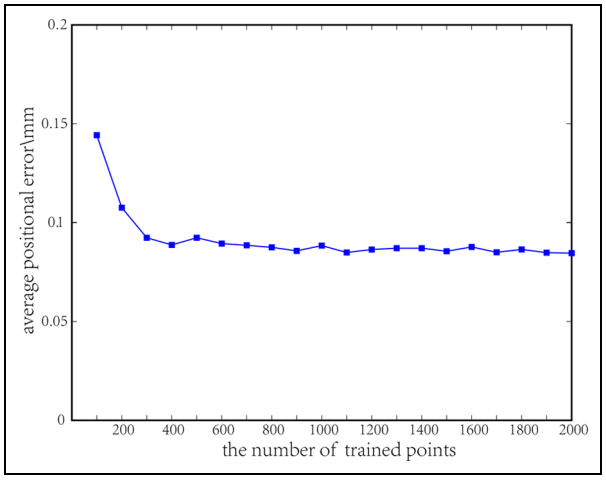

Figure 9. Effect of the number of the nodes in the hidden layer on the average position error.

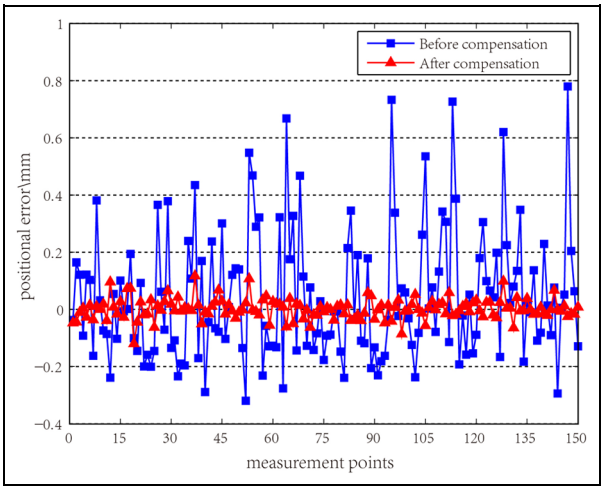

Figure 10. Positional errors on the *X* axis of robot TCP.

From Figures 8 and 9, if the number of nodes in the hidden layer is less than 20, the maximum positional error and average positional error all have a negative correlation with the number of nodes. If the number of nodes is greater than 20, the maximum positional error and average positional error are nearly equivalent to a constant.

The calculations and computation time will increase as the number of nodes in the hidden layer increases. The experimental results show that choosing the appropriate number of nodes in the hidden layer for the ELM can increase the computational efficiency without decreasing the high absolute position accuracy.

Positional error compensation

To verify the effectiveness of the compensation method in this article, experiments were conducted on an aviation drilling robot. In practice, the position accuracy of holes is basically determined by the maximum positional error rather than the average positional error. Hence, when the average positional errors with difference parameters are nearly consistent, the minimum maximum positional error is optimal. Figures 6 and 7 show that when the number of training points is greater than 300, the average position error tends to be stable. When the number of training points is 1000, the maximum positional error is minimum. Similarly, Figures 8 and 9 show that when the number of nodes is 40, the maximum positional error is minimum.

Thus, the data of 1000 random points from the 2000 points mentioned above are chosen to train the ELM. The hidden layer is composed of 40 neurons. A sum function is used as the activating function of the ELM.

After an ELM is constructed, 150 random points in the robot workspace are chosen to verify the compensation method. The positional errors of 150 random points are measured before and after compensation. The experimental results of positional errors of 150 measurement points before and after compensation are shown in Figures 10–12. The histograms of positional errors along the *X*, *Y*, and *Z* axes before and after compensation are described in Figures 13–15. The detailed statistical results of the positional errors are shown in Table 1. According to the experimental results, the positional errors on the *X*, *Y* and *Z* axes after compensation in the error range and average errors are less

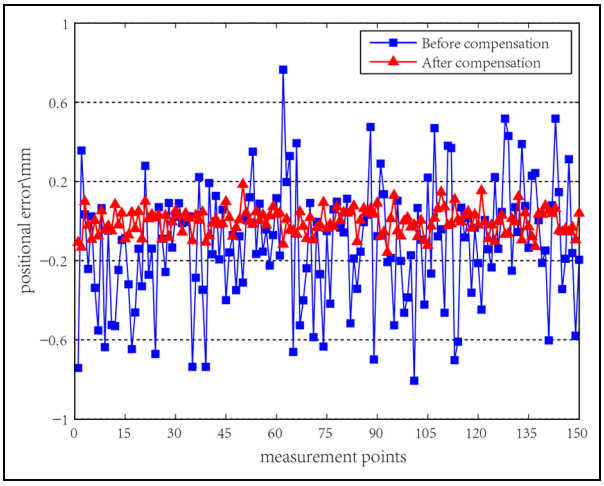

Figure 11. Positional errors on the *Y* axis of robot TCP.

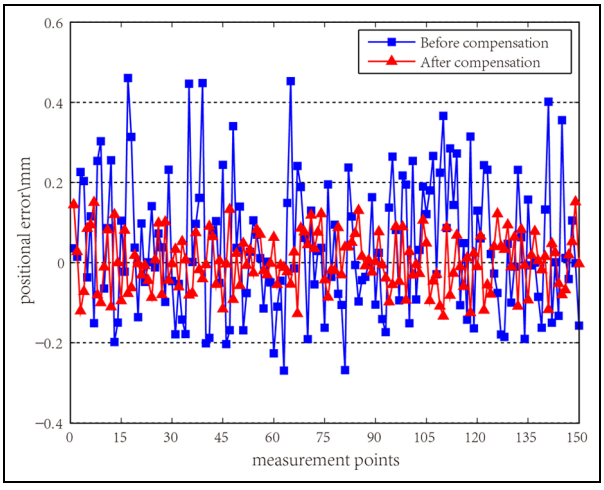

Figure 12. Positional errors on the *Z* axis of robot TCP.

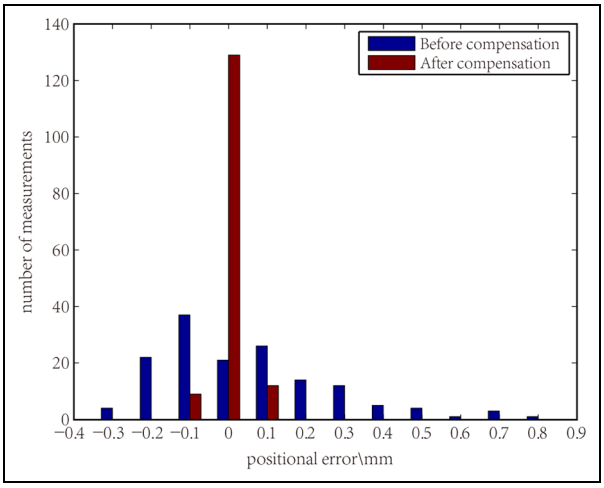

Figure 13. Histogram of positional errors along the *X* axis.

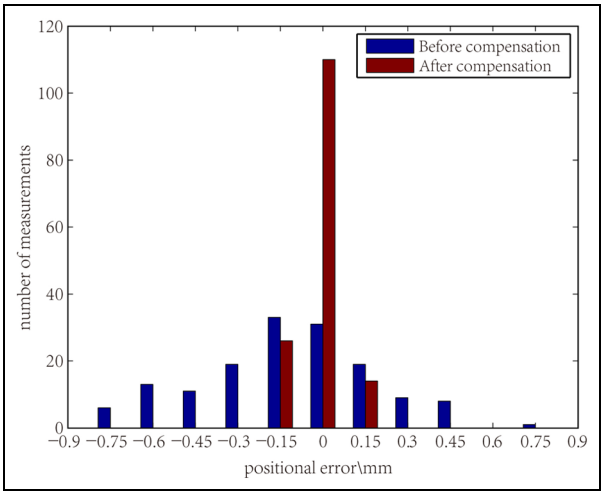

Figure 14. Histogram of positional errors along the *Y* axis.

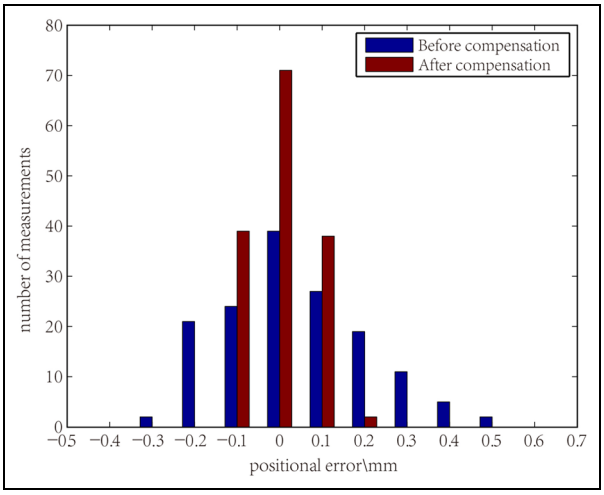

Figure 15. Histogram of positional errors along the *Z* axis.

than the positional errors before compensation. The experimental results show that the proposed compensation method can enhance the position accuracy of aviation drilling robot in aircraft assembly.

To verify the high accuracy and high efficiency of the proposed method, three methods, which are referred to as method 1,[33] method 2,[16] and method 3,[15] are compared with the proposed method. Method 1 and method 2 were all model-free methods and they used the error similarity to estimate the positional errors of sampled points. Method 3, a traditional model-based method, developed the kinematic model of robot and identified the parameters of kinematic model. Figures 16 and 17 and Table 2 summarize the compensation results of four methods. The results show that the proposed method achieves higher position accuracy than the rest methods. The validation results also show that the average absolute positional

Table 2. The absolute positional errors of drilling robot by four methods.

	Range (mm)	Mean (mm)	Standard deviation (mm)
Before compensation	[0.0851, 1.0207]	0.3816	0.2119
Method 1	[0.0354, 0.6301]	0.2061	0.1135
Method 2	[0.0172, 0.5309]	0.1505	0.0936
Method 3	[0.0144, 0.3416]	0.1113	0.0605
Proposed method	[0.0119, 0.1946]	0.0920	0.0411

Table 3. The results of running time.

	Method 1	Method 2	Method 3	Proposed method
Time (s)	0.1459	1.3459	184.9542	0.0251

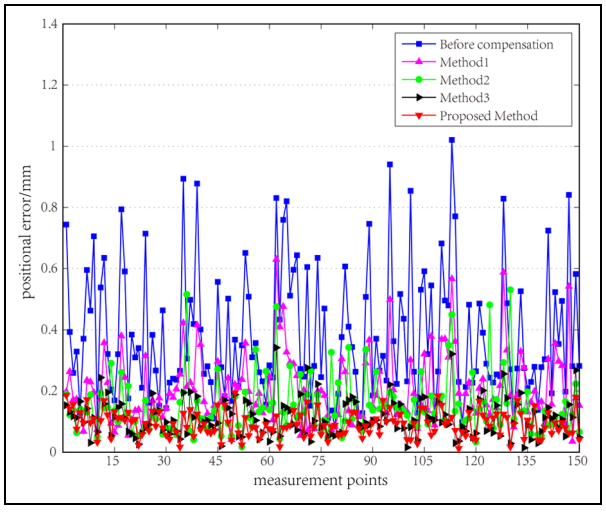

Figure 16. The absolute positional errors of drilling robot after compensation for four methods.

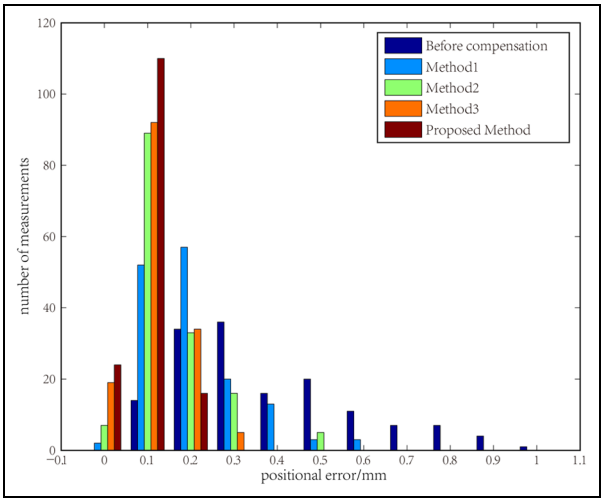

Figure 17. Histogram of absolute positional errors after compensation for four methods.

errors before and after compensation are 0.3816 and 0.0920 mm, respectively. The maximum values before and after compensation are 1.0207 and 0.1946 mm, respectively. The average and maximum absolute position accuracies of the robot TCP are improved by 75.89% and 80.93%, respectively. From the experimental results, the compensation method in this article can meet the position accuracy requirement of an aviation drilling robot in aircraft assembly.

The four methods are programmed in MATLAB running on a Windows computer with a 2.6-GHz Intel Core i7-6700HQ CPU and 8 GB RAM. Table 3 shows the running time for training or parameter identification to estimate the positional errors of 150 sample points based on the three methods. Table 3 shows that method 3 requires more time than the other methods. The running times of method 1 and method 2 are almost 6 times and 54 times that of the proposed method, respectively. The results demonstrate that the proposed method has the advantages of low computational complexity and high efficiency.

Conclusion

A compensation method based on the ELM model for an aviation drilling robot was proposed to enhance the absolute position accuracy and solve the problem of complex modeling and computational complexity in the traditional compensation method.

1. The influence of the geometric factors and the non-geometric factors of the aviation drilling robot is considered in the compensation method based on the ELM model. The theoretical position and positional errors measured by a high-precision laser tracker were the input training data and output training data used to train and

construct the ELM model. The ELM could predict the positional errors of the prediction points. The drilling robot controller compensated for the predicted positional errors.

2. To verify the effectiveness of the proposed compensation method in real applications, experimental compensation was conducted on an aviation drilling robot. After error compensation, the average absolute positional errors were improved from 0.3816 to 0.0920 mm, and the maximum values improved from 1.0207 to 0.1946 mm. The experimental results showed that the compensation method in this article can improve the absolute position accuracy for an aviation drilling robot, has the advantages of low computational complexity and high efficiency, and meets the requirements of aircraft assembly.
3. The number of training points and the nodes in the hidden layer for the ELM were two important factors influencing the absolute position accuracy of a drilling robot. To obtain the relationship between the absolute position accuracy and the two factors, a series of experiments were conducted on an aviation drilling robot. The experimental results demonstrated that choosing the appropriate number of training points and hidden neurons for the ELM can ensure high absolute position accuracy and reduce the time and amount of work.

Declaration of conflicting interests

The author(s) declared no potential conflicts of interest with respect to the research, authorship, and/or publication of this article.

Funding

The author(s) disclosed receipt of the following financial support for the research, authorship, and/or publication of this article: This research is partially supported by the National Natural Science Foundation of China (no. 61375085) and the Foundation of Shanghai Aircraft Manufacturing Co., Ltd (no. 32284001).

References

1. Yu L, Zhang YL, Wang YH, et al. Research status of aircraft automatic drilling and riveting system and its key technology. *Aeronaut Manuf Technol* 2017; 9: 16–25.
2. Zhu W, Qu W, Cao L, et al. An off-line programming system for robotic drilling in aerospace manufacturing. *Int J Adv Manuf Tech* 2013; 68: 2535–2545.
3. Bi S and Liang J. Robotic drilling system for titanium structures. *Int J Adv Manuf Tech* 2011; 54: 767–774.
4. Wang M, Xue SD, Chen WD, et al. One-side pressed burrless drilling technology for aircraft automatic assembly. *Aeronaut Manuf Technol* 2011; 9: 26–29.
5. Hong P, Tian W and Mei DQ. Robots' accuracy compensation technique based on variable parameters using space grids. *Robot* 2015; 3: 327–335.
6. Frommknecht A, Kuehnle J, Effenberger I, et al. Multisensor measurement system for robotic drilling. *Robot Cim-Int Manuf* 2017; 47: 4–10.
7. Joubair A and Bonev IA. Kinematic calibration of a six-axis serial robot using distance and sphere constraints. *Int J Adv Manuf Tech* 2015; 77: 515–523.
8. Wang D and Chi J. A survey of kinematic calibration of robot. *Appl Res Comput* 2007; 24: 8–11.
9. Du G, Shao H, Chen Y, et al. An online method for serial robot self-calibration with CMAC and UKF. *Robot Cim-Int Manuf* 2016; 42: 39–48.
10. Kamali K, Joubair A, Bonev IA, et al. Elasto-geometrical calibration of an industrial robot under multidirectional external loads using a laser tracker. In: *Proceeding of IEEE international conference on robotics and automation*, Stockholm, 16–21 May 2016, pp.4320–4327. New York: IEEE.
11. Albert N, Mohamed S, Ahmed J, et al. Comparison of two calibration methods for a small industrial robot based on an optical CMM and a laser tracker. *Robotica* 2014; 32: 447–466.
12. Zhong XL, Lewis JM and Francis LNN. Autonomous robot calibration using a trigger probe. *Robot Auton Syst* 1996; 18: 395–410.
13. Judd RP and Knasinski AB. A technique to calibrate industrial robots with experimental verification. *IEEE T Robotic Autom* 1990; 6: 20–30.
14. Nubiola A and Bonev IA. Absolute calibration of an ABB IRB 1600 robot using a laser tracker. *Robot Cim-Int Manuf* 2013; 29: 236–245.
15. Nguyen HN, Zhou J, Kang HJ, et al. A calibration method for enhancing robot accuracy through integration of an extended Kalman filter algorithm and an artificial neural network. *Neurocomputing* 2015; 151: 996–1005.
16. Zeng Y, Tian W and Liao W. Positional error similarity analysis for error compensation of industrial robots. *Robot Cim-Int Manuf* 2016; 42: 113–120.
17. Abderrahim M and Whittaker AR. Kinematic model identification of industrial manipulators. *Robot Cim-Int Manuf* 2000; 16: 1–8.
18. Whitney DE, Lozinski CA and Rourke JM. Industrial robot forward calibration method and results. *J Dyn Syst: T ASME* 1986; 108: 1–8.
19. Gatti G and Danieli G. A practical approach to compensate for geometric errors in measuring arms: application to a six-degree-of-freedom kinematic structure. *Meas Sci Technol* 2008; 19: 15107.
20. Stone HW and Sanderson AC. Statistical performance evaluation of the S-model arm signature identification technique. In: *Proceeding of IEEE international conference on robotics and automation*, Philadelphia, PA, 24–29 April 1988, pp.939–946. New York: IEEE.
21. Stone H, Sanderson A and Neuman C. Arm signature identification. In: *Proceeding of IEEE international conference on robotics and automation*, San Francisco, CA, 7–10 April 1986, pp.41–48. New York: IEEE.

22. Bai Y, Cong M, Yang X, et al. Kinematic parameter identification for 6R serial robots based on a 6-parameter model. *Robot* 2015; 37: 486–492.
23. Chen I, Yang G, Tan C, et al. Local POE model for robot kinematic calibration. *Mech Mach Theory* 2001; 36: 1215–1239.
24. He R, Zhao Y, Yang S, et al. Kinematic-parameter identification for serial-robot calibration based on POE formula. *IEEE T Robot* 2010; 26: 411–423.
25. Joubair A, Zhao LF, Bigras P, et al. Absolute accuracy analysis and improvement of a hybrid 6-DOF medical robot. *Ind Robot* 2015; 42: 44–53.
26. Wu H, Tizzano W, Andersen TT, et al. Hand-eye calibration and inverse kinematics of robot arm using neural network. *Adv Intell Syst* 2014; 581–591.
27. Omodei A, Legnani G and Adamini R. Three methodologies for the calibration of industrial manipulators: experimental results on a SCARA robot. *J Field Robot* 2000; 17: 291–307.
28. Fassi I, Legnani G, Tosi D, et al. Calibration of serial manipulators: theory and applications. In: Huat LK (ed.) *Industrial robotics: programming, simulation and applications*. London: InTech, 2006, pp.147–170.
29. Park IW, Lee BJ, Cho SH, et al. Laser-based kinematic calibration of robot manipulator using differential kinematics. *IEEE/ASME T Mech* 2012; 17: 1059–1067.
30. Santolaria J, Conte J and Ginés M. Laser tracker-based kinematic parameter calibration of industrial robots by improved CPA method and active retroreflector. *Int J Adv Manuf Tech* 2013; 66: 2087–2106.
31. Alici G and Shirinzadeh B. A systematic technique to estimate positioning errors for robot accuracy improvement using laser interferometry based sensing. *Mech Mach Theory* 2005; 40: 879–906.
32. Alıcı G, Jagielski R, Şekercioğlu YA, et al. Prediction of geometric errors of robot manipulators with particle swarm optimisation method. *Robot Auton Syst* 2006; 54: 956–966.
33. Tian W, Zeng Y, Zhou W, et al. Calibration of robotic drilling systems with a moving rail. *Chinese J Aeronaut* 2014; 27: 1598–1604.
34. Aoyagietal S. Improvement of robot accuracy by calibrating kinematic model using a laser tracking system-compensation of non-geometric errors using neural networks and selection of optimal measuring points using genetic algorithm-. In: *Proceedings of IEEE/international conference on intelligent robots and systems*, Taipei, Taiwan, 18–22 October 2010, pp.5660–5665. New York: IEEE.
35. Wang D, Bai Y and Zhao J. Robot manipulator calibration using neural network and a camera-based measurement system. *T I Meas Control* 2010; 34: 105–121.
36. Rui MA, Yushu L and Yanhui D. An intrusion detection method based on neural network expert system. *Comput Eng Appl* 2004; 40: 151–153.
37. Huang GB, Zhu QY and Siew CK. Extreme learning machine: a new learning scheme of feedforward neural networks. In: *Proceeding of IEEE international joint conference on neural networks,* Budapest, 25–29 July 2004, pp.985–990. New York: IEEE.
38. Huang GB, Zhu QY and Siew CK. Extreme learning machine: theory and applications. *Neurocomputing* 2006; 70: 489–501.
39. Yang C, Huang K, Cheng H, et al. Haptic identification by ELM-controlled uncertain manipulator. *IEEE T Syst Man Cyb* 2017; 47: 2398–2409.